ISSN 1064-2269, Journal of Communications Technology and Electronics, 2017, Vol. 62, No. 7, pp. 809–819. © Pleiades Publishing, Inc., 2017.
Original Russian Text © E.T. Dilmieva, A.V. Irzhak, A.P. Kamantsev, V.V. Koledov, V.G. Shavrov, R.M. Grechishkin, E.P. Krasnoperov, V.A. Dikan, F. Albertini, S. Fabbrici, L. González-Legarreta, B. Hernando, 2017, published in Radiotekhnika i Elektronika, 2017, Vol. 62, No. 7, pp. 703–713.

NANOELECTRONICS

Rapidly Quenched Ferromagnetic Ribbons with Shape Memory for Magnetically Controlled Micromechanic Devices

E. T. Dilmieva[a, b, c, *], A. V. Irzhak[d, e], A. P. Kamantsev[a, b], V. V. Koledov[a, b], V. G. Shavrov[a], R. M. Grechishkin[f], E. P. Krasnoperov[g], V. A. Dikan[a, d], F. Albertini[h], S. Fabbrici[h], L. González-Legarreta[i], and B. Hernando[i]

[a] *Kotel'nikov Institute of Radio Engineering and Electronics, Russian Academy of Sciences, Moscow, 125009 Russia*
[b] *International Laboratory of High Magnetic Fields and Low Temperatures, 53-421 Wroclaw, Poland*
[c] *Bauman State Technical University, Moscow, 105005 Russia*
[d] *Moscow Institute of Steel and Alloys, National Research Technological University, Moscow, 119049 Russia*
[e] *Institute of Microelectronic Technology and Ultrahigh-Purity Materials, Russian Academy of Sciences, Chernogolovka, Moscow oblast, 142432 Russia*
[f] *Tver State University, Tver, 170100 Russia*
[g] *Kurchatov Institute, National Research Center, Moscow, 123182 Russia*
[h] *Institute of Materials for Electronics and Magnetism, 43124 Parma, Italy*
[i] *Faculty of Physics, University of Oviedo, 33005 Oviedo, Spain*
**e-mail: kelvit@mail.ru*

Received June 20, 2016

Abstract—One-way shape-memory effect (SME) controlled by temperature and magnetic field in rapidly melt-quenched (RMQ) Heusler-alloy ($Ni_{53}Mn_{24}Ga_{23}$) ribbons is experimentally studied. Two-way SME that results from training is demonstrated for submicron $Ni_{53}Mn_{24}Ga_{23}$ samples. Reversible thermally and magnetically controlled bending of no less than 1.5% and deflection of no less than 2 μm are reached for composite $Ni_{53}Mn_{24}Ga_{23}$/Pt microactuators with sizes of $25 \times 2.3 \times 1.7$ μm^3 in the presence of magnetic field of $\mu_0 H = 8$ T at an initial temperature of 63°C.

DOI: 10.1134/S106422691707004X

INTRODUCTION

Recent progress in modern technologies is based on a search for novel materials with specific combinations of physical and functional properties, in particular, materials that exhibit shape and size variations due to thermoelastic structural martensite transition in the presence of external effects (e.g., mechanical stress, magnetic field, ultrasound, and temperature). Functional materials with such properties may serve as unique materials in microsystem technology, medicine, and alternative power engineering. There has been considerable recent interest in functional intermetal alloys with the effect of giant magnetic strain [1]. Several Heusler ferromagnetic alloys exhibit thermoelastic martensite transition and magnetically controlled shape-memory effect (SME) (e.g., Ni–Mn–In, Ni–Mn–Ga, Ni–Mn–Sb, Ni—Mn–Sn, and Ni–Mn–In–Co alloys) [2–14].

The Ni–Mn–Ga Heusler alloy exhibits developed SME effect [15–19]. For example, single crystals of the Ni–Mn–Ga alloy exhibit reversible strains of up to 10% in the presence of magnetic fields of up to 10 kOe whereas the strain is 0.3% for the TbFe alloy with the giant magnetostriction. The properties of the Heusler alloys are well studied for samples that represent polycrystalline ingots, single crystals, rapidly quenched ribbons, and granules. It is known that rapidly quenched Ni–Mn–Ga ribbons may be mechanically stable and may have good parameters of the martensite transition (temperature that is close to room temperature and relatively narrow temperature hysteresis). Thus, the ribbons are promising for applications in sensor and actuator technologies [20–26].

In spite of significantly different physical properties, the Heusler alloys exhibit several common features. In particular, the phase transitions in Ni–Mn–Sn, Co–Ni–Al, Ni–Mn–In, and Ni–Mn–Ga Heusler alloys are extremely sensitive to the chemical composition and the properties of such alloys strongly depend on external fields [27–40]. Note insufficient data on phase transitions and giant strains induced by variations in temperature and magnetic field in samples with micro- and nanoscale sizes.

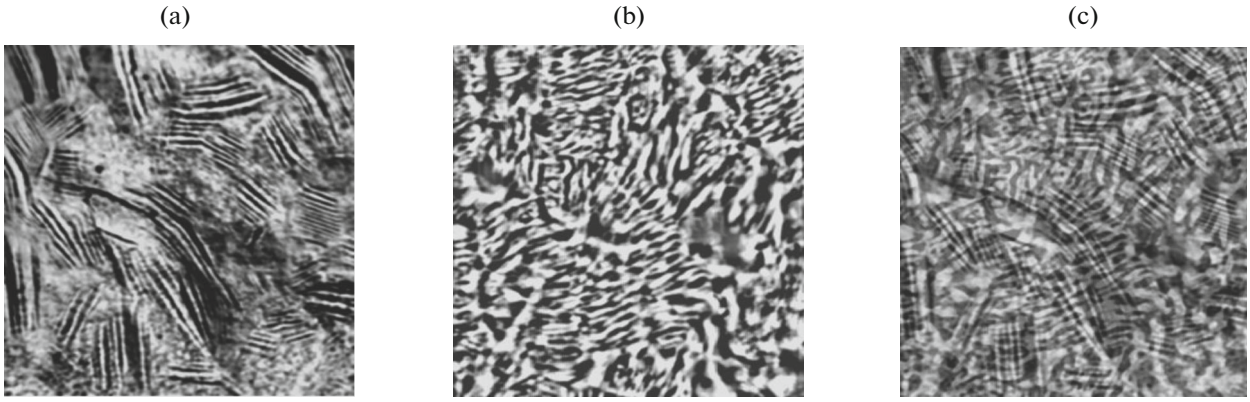

Fig. 1. Microphotographs of the ferromagnetic domain structure of the $Ni_{53}Mn_{24}Ga_{23}$ Heusler-alloy ribbon annealed over 72 h: (a) martensite relief, (b) magnetic domains and (c) combined images of both structures.

The purpose of this work is the analysis of SME in rapidly quenched ribbons of the $Ni_{53}Mn_{24}Ga_{23}$ Heusler alloy and layered composites with micron and submicron sizes based on such ribbons with allowance for variations in temperature and magnetic field.

1. EXPERIMENTAL

1.1. Samples of $Ni_{53}Mn_{24}Ga_{23}$ Rapidly Quenched Alloy

Samples of $Ni_{53}Mn_{24}Ga_{23}$ rapidly quenched alloy are fabricated with the aid of spinning [41]. The quenching rate is 10^7 °C/s. The ribbons are cut into fragments with a length of 1–10 cm. Each fragment is annealed in vacuum at a temperature of 800°C over 72 h. The Curie temperature and the starting and final temperatures of the austenite–martensite and martensite–austenite transitions (M_s, M_f, A_s, A_f) are determined using the differential scanning calorimetry: $M_s = 49.5$°C, $M_f = 41.2$°C, $A_s = 50.4$°C, $A_f = 60.7$°C, and $T_C = 72.5$°C. Fabrication technology and the results on physical properties of the ribbons depending on parameters of preliminary thermal processing can be found in [41–44] (see also Fig. 1).

1.2. Submicron Samples

Submicron $Ni_{53}Mn_{24}Ga_{23}$ samples that represent thin plates fixed at one end (consoles) are fabricated and studied using a setup for selective ion etching (FEI STRATA FIB 201 ion scanning microscope) equipped with an Omniprobe nanomanipulator and diode laser for heating of samples and the SME study. (The technology of focused ion beam (FIB) is comprehensively characterized in [45].) Figure 2 illuistrates fabrication of submicron samples of the $Ni_{53}Mn_{24}Ga_{23}$ alloy: the microphotograph (Fig. 2a) shows the surface of the rapidly melt-quenched (RMQ) ribbon that is used to make the console sample (Fig. 2b). The method for fabrication of submicron samples consists of the soldering and training stages. The sample is soldered to the end of the microwire of the Omniprobe nanomanipulator with the aid of the Pt layer that is obtained using the ion-stimulated vapor deposition. Then, the training is performed using mechanical bending (Figs. 2c and 2d). Typical sizes of the samples under study are (10–20) × (2–3) × (0.3–1) μm^3.

Note that the photographs obtained with the aid of the FIB setup (Fig. 2b) clearly show martensite twins (cross sections of the 3D structure). The twins are formed due to ion etching and can be detected using ion microscopy (Fig. 3).

1.3. Composites with SME Based on $Ni_{53}Mn_{24}Ga_{23}$

1.3.1. Physical principles of the composite actuator. The composite actuator with SME [43, 44] contains two layers (elastic and SME layers) as a conventional bimetal plate does. Note that the SME element is preliminary pseudoplastically deformed (e.g., stretched).

The physical effect of the pseudoplastic deformation of the SME alloy can be interpreted in a way as follows. The temperature of the austenite–martensite transition increases in the presence of a significant external mechanical stress. Martensite is generated in such a sample upon cooling from the austenite state via the phase-transition point. The generation is primarily initiated in regions with the maximum strain. Appropriately oriented variants (stretched or compressed along the tension and compression axes) are predominantly generated. Thus, the pseudoplastic deformation is the state of sample in which microscopic variation in shape and/or size is reached in the martensite state owing to the generation of martensite variants with appropriate orientations of crystallographic axes.

We assume that the composite containing elastic layer that is rigidly connected with the preliminary pseudoplastically extended (in the martensite state) SME layer is heated prior to the termination of the martensite–austenite transition. Martensite twins vanish in such composite and mechanical compres-

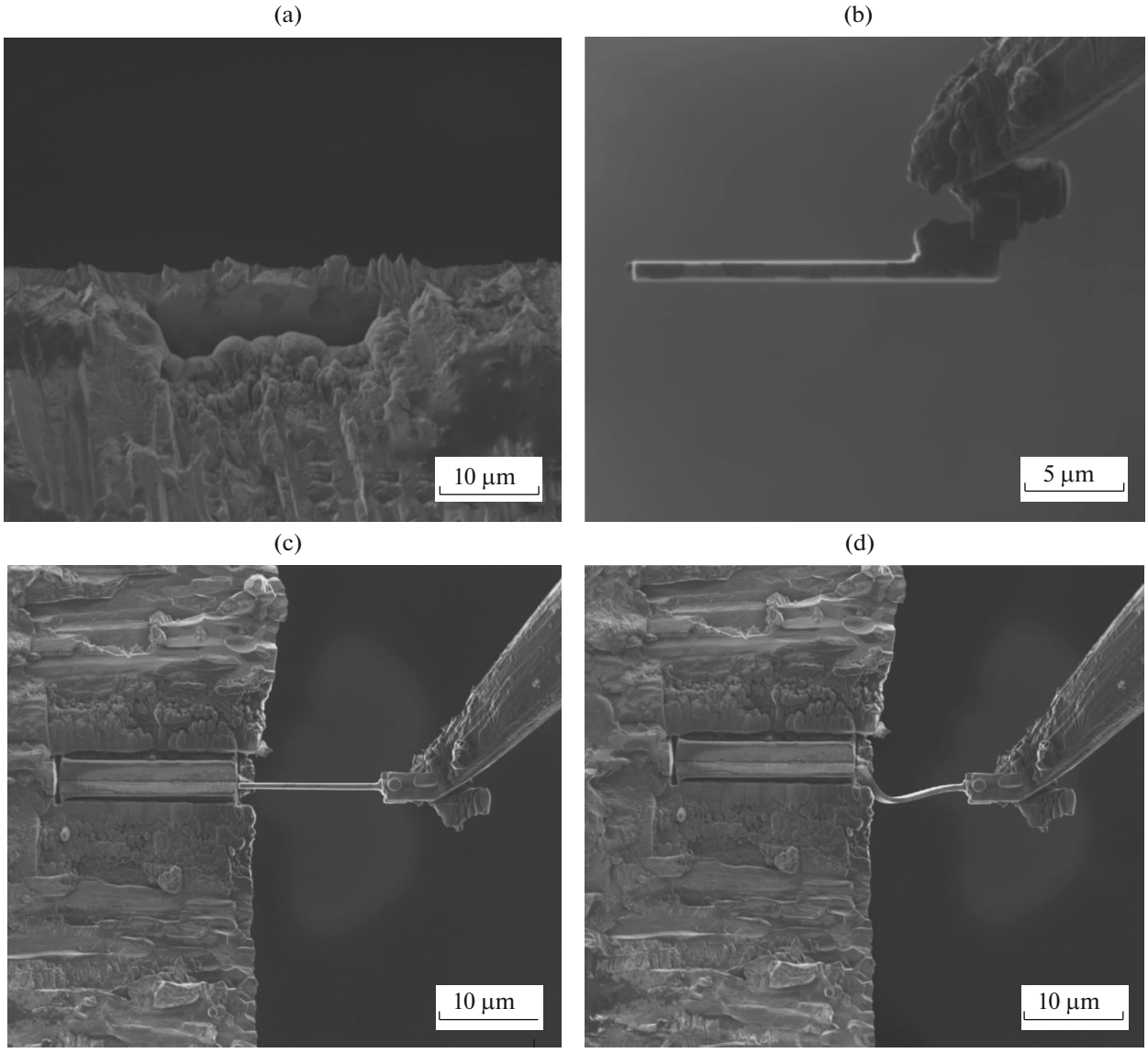

Fig. 2. Microphotographs that illustrate the SME training of submicron samples of the $Ni_{53}Mn_{24}Ga_{23}$ Heusler alloy: (a) edge of ribbon, (b) prototype of actuator, (c) prior to deformation and (d) after deformation.

sion emerges. The compression of one layer of the bimorph composite causes stretching of the elastic (passive) layer and, hence, bending of the composite as a whole. When the temperature becomes lower than the martensite transition point, the elastic layer causes pseudoplastic stretching of the SME layer that exhibits the martensite transition. Thus, the SME layer appears to be pseudoplastically extended and the initial linear shape of the composite is restored.

Note that the controlled bending of the composite with SME is greater than the bending of a conventional bimetal plate by several orders of magnitude and is greater than the bending of the material with two-way shape memory by at least an order of magnitude. In practice, the controlled deformation of the bimorph composite is limited by strength parameters of the elastic layer. The application of such an efficient system with preliminary stressed composites with SME allows new functional solutions and provides quantitative improvement of existing devices. We choose the composite actuator, since the corresponding technology makes it possible to fabricate a device with extremely small sizes. We only make assumptions on the limiting sizes of the composite microactuator with SME, since the physical limits of the manifestation of the martensite transition and SME related to the size of the alloy sample remain unknown.

1.3.2. Fabrication of microsamples of the $Ni_{53}Mn_{24}Ga_{23}$/Pt composites. A detailed procedure of the fabrication of composite SME microactuators based on rapidly quenched Ti_2NiCu alloys can be found in [41]. Several specific features of the process

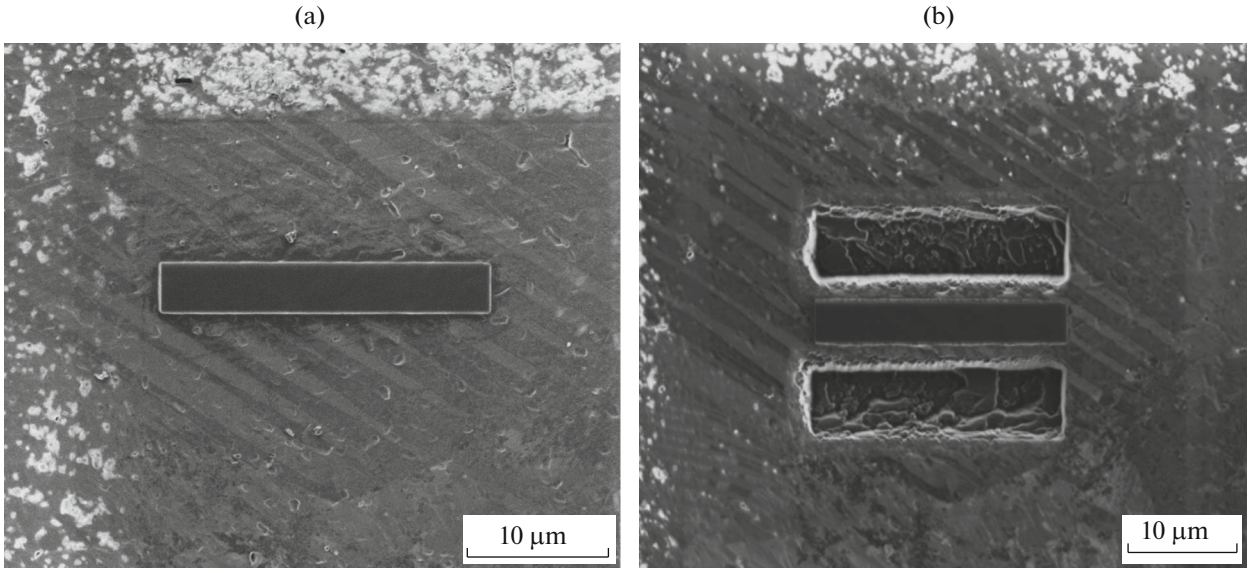

Fig. 3. Microphotographs that illustrate fabrication of the $Ni_{53}Mn_{24}Ga_{23}$/Pt composites: (a) Pt deposition on the surface of the rapidly quenched alloy and (b) etching of the $Ni_{53}Mn_{24}Ga_{23}$/Pt bar on two sides with the aid of the ion beam.

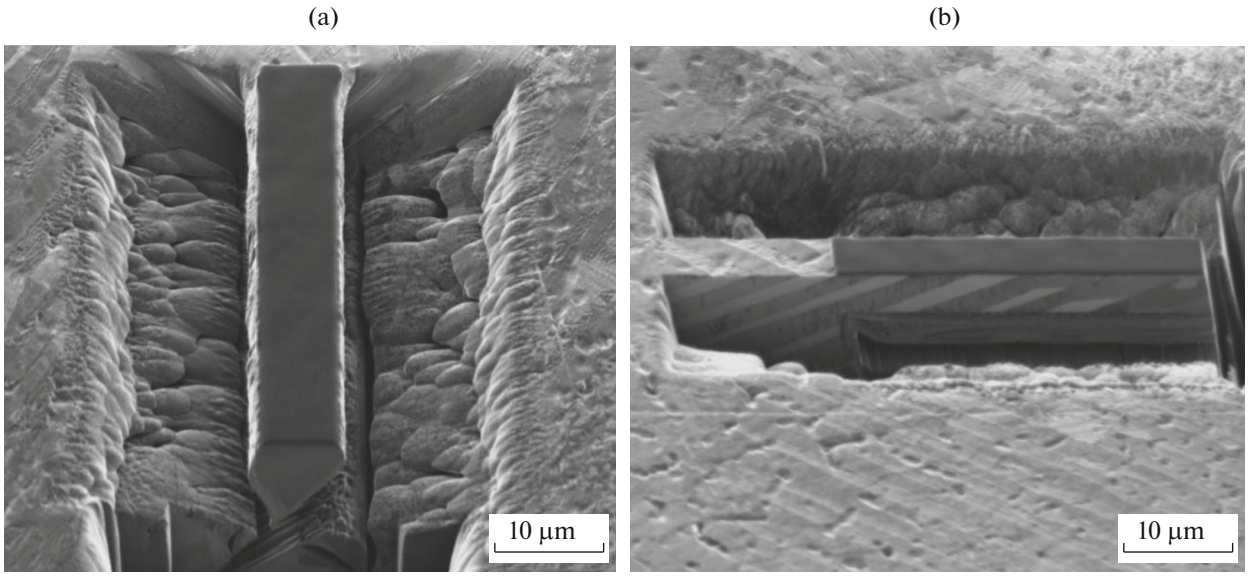

Fig. 4. Microphotographs that illustrate fabrication of the $Ni_{53}Mn_{24}Ga_{23}$/Pt composites: (a) etching of channels under composite at an angle of 45° on both sides and (b) view at an angle of 45° (note the presence of martensite domains).

must be taken into account for the $Ni_{53}Mn_{24}Ga_{23}$ alloy [8, 18, 46, 47]. The procedure consists of several stages. At the first stage, a ribbon with a thickness of 30–40 μm is produced with the aid of rapid melt-quenching. At the second stage, the pseudoplastic tension is induced in the alloy. Then, a thin rectangular Pt layer is deposited on the cleaned surface of the RMQ alloy with SME using ion-stimulated deposition to form the elastic layer (Fig. 3a). The longer side of the rectangle is parallel to the stretching axis. A composite beam is cut from the volume of the alloy ribbon (Fig. 3b). The microsample is obtained with the aid of etching of the surface of alloy at an angle of 45° on both sides of the rectangular Pt stripe (Figs. 4a and 4b). Finally, the Omniprobe manipulator (Fig. 5) is used to transport the composite and fix it on the end surface of the silicon substrate (Fig. 6).

2. EXPERIMENTAL PROCEDURE

2.1. One-way SME in the Presence of Thermal and Magnetic Fields

The thermomechanical properties of rapidly quenched $Ni_{53}Mn_{24}Ga_{23}$ ribbons are studied using the method that is based on the application of a ridged

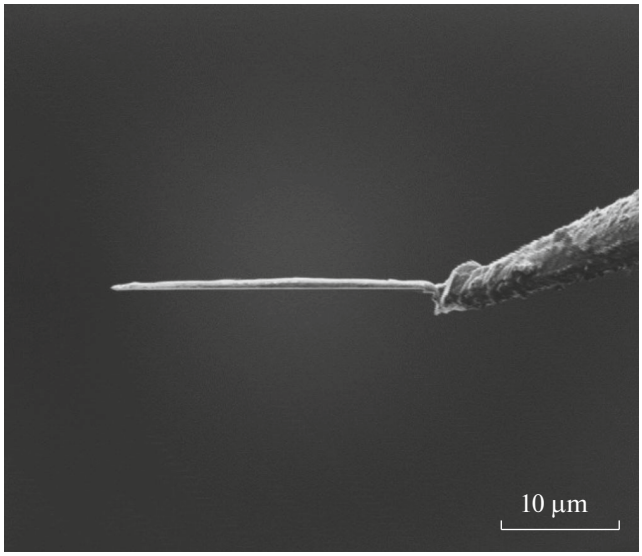

Fig. 5. Transportation of the prototype of microactuator using the Omniprobe manipulator for fixing on silicon plate.

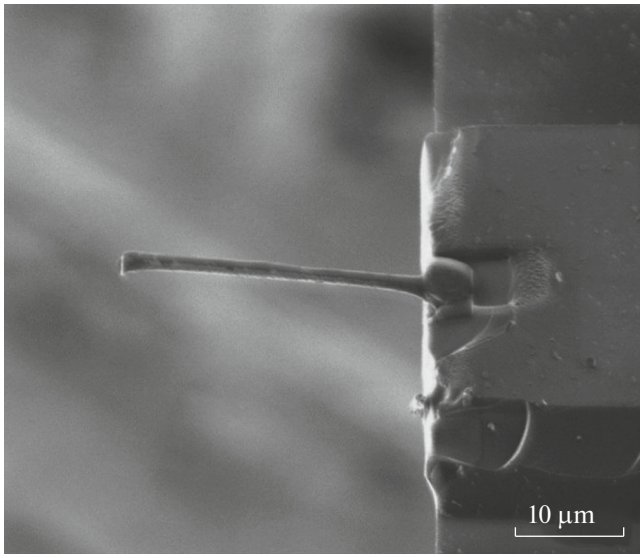

Fig. 6. Microactuator fixed on the silicon plate using the ion-stimulated deposition of Pt.

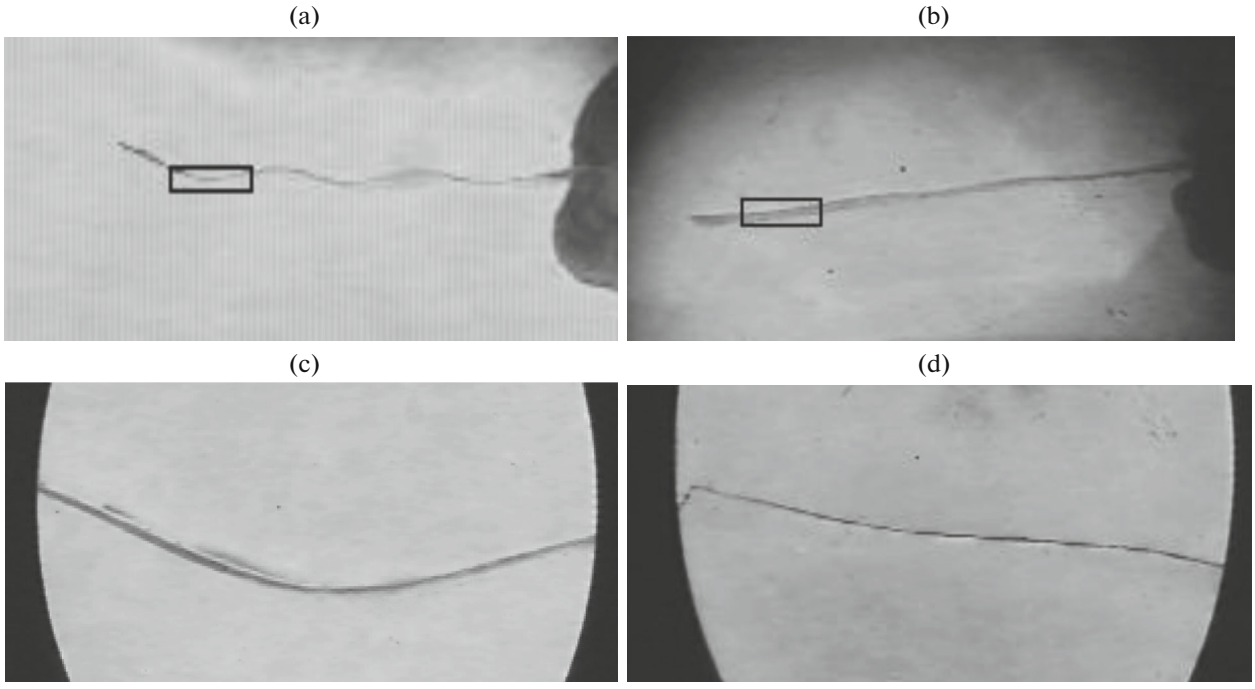

Fig. 7. (a) and (c) Pseudoplastic bending of the rapidly quenched $Ni_{53}Mn_{24}Ga_{23}$ alloy ribbon in the ridged press due to austenite–martensite transition and (b) and (d) recovery of the original linear shape after heating.

press [41] that exerts pressure at several points and makes it possible to fabricate a wave-shaped sample (Figs. 7a–7d).

The initially linear ribbon in the austenite state is placed into the ridged press. The external pressure is provided by a spring or weight that presses the upper part to the lower part. The bending of the ribbon is estimated using the measured displacement of the ridges. When the temperature of the press with the sample becomes lower than the starting point of the martensite transition M_S, the ribbon is strongly deformed. In the presence of external force, the shape is recovered when the temperature exceeds point A_F. Thus, the one-way SME is observed. It is known that

(a) (b)

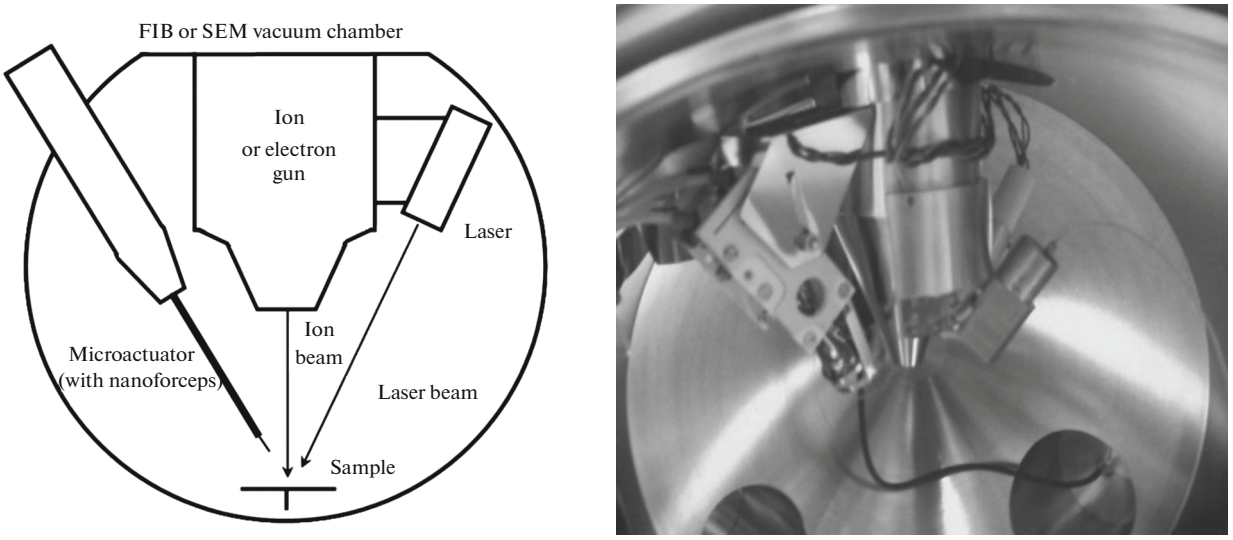

Fig. 8. (a) Experimental scheme for the SME study in submicron samples of the $Ni_{53}Mn_{24}Ga_{23}$ alloy and (b) photograph of the working chamber of the FEI STRATA 201 FIB ion microscope.

relative deformation ε upon bending of a thin ribbon (compression and stretching at the inner and outer surfaces, respectively) is related to radius of curvature R and thickness h:

$$\varepsilon = h/2R. \quad (1)$$

The cylindrical shape of the press limits the curvature of ribbon at the point of maximum bending and, hence, protects the fragile ribbon against breaking in experiments. The magnetically controlled SME is studied in the presence of the fields of up to 8 T. The measurement system with the ridged press made of nonmagnetic materials is placed in the Bitter solenoid.

2.2. SME in the $Ni_{53}Mn_{24}Ga_{23}$ Submicron Samples

The SME in the $Ni_{53}Mn_{24}Ga_{23}$ submicron samples is studied using the FEI STRATA 201 FIB ion microscope with the Omniprobe nanomanipulator and diode laser placed in the working chamber of the ion microscope (Fig. 8). The sample attached to the end of the Omniprobe nanomanipulator is placed in the chamber of the ion microscope. The radiation of the diode laser is used for heating [8].

2.3. Thermally Controlled SME in the $Ni_{53}Mn_{24}Ga_{23}$/Pt Composite Sample

In the experiments on the thermally controlled SME, the composite sample is placed in optical microscope (Fig. 9) equipped with a heater and thermocouple. The heating leads to bending, and cooling makes it possible to restore the original (linear) shape of the sample. The process is detected using a digital camera, and the images are used to determine the curvature of actuator versus temperature. Then, the relative deformation is calculated with the aid of formula (1).

2.4. Magnetically Controlled SME in the $Ni_{53}Mn_{24}Ga_{23}$/Pt Composite Sample

The results of [13] show that the SME in the $Ni_{53}Mn_{24}Ga_{23}$ alloy is possible in the presence of relatively strong magnetic fields. The needed magnetic field is determined by two parameters: field sensitivity of the martensite transition (slope of the dependence of temperature of the martensite transition on the field (dT_M/dH) and width of the temperature hysteresis of the martensite transition (ΔT_M). Quantity dT_M/dH is calculated using the Clapeyron– Clausius formula

$$dT_M/dH = -\Delta MT/\lambda, \quad (2)$$

where ΔM is the variation in the magnetization of alloy due to the transition, T_M is the mean transition temperature, and λ is the latent heat. For the $Ni_{53}Mn_{24}Ga_{23}$ alloy, derivative dT/dH is about 0.8°C/T and the temperature hysteresis of the martensite transition is ΔT = 6–8°C. Thus, the needed magnetic field is 8–10 T. Such a field can be generated only with the aid of Bitter solenoids or superconducting magnets. In the experiments, we use Bitter solenoids of the International Laboratory of High Magnetic Fields and Low Temperatures (Wroclaw, Poland) [48] (Fig. 9). The actuator is placed on a table and irradiated using two LEDs. The motion of the actuator is monitored with the aid of a specific optical microscope made of nonmagnetic materials. In the presence of the magnetic field, the magnetically controlled SME is detected using a video camera. Then, we determine the relative

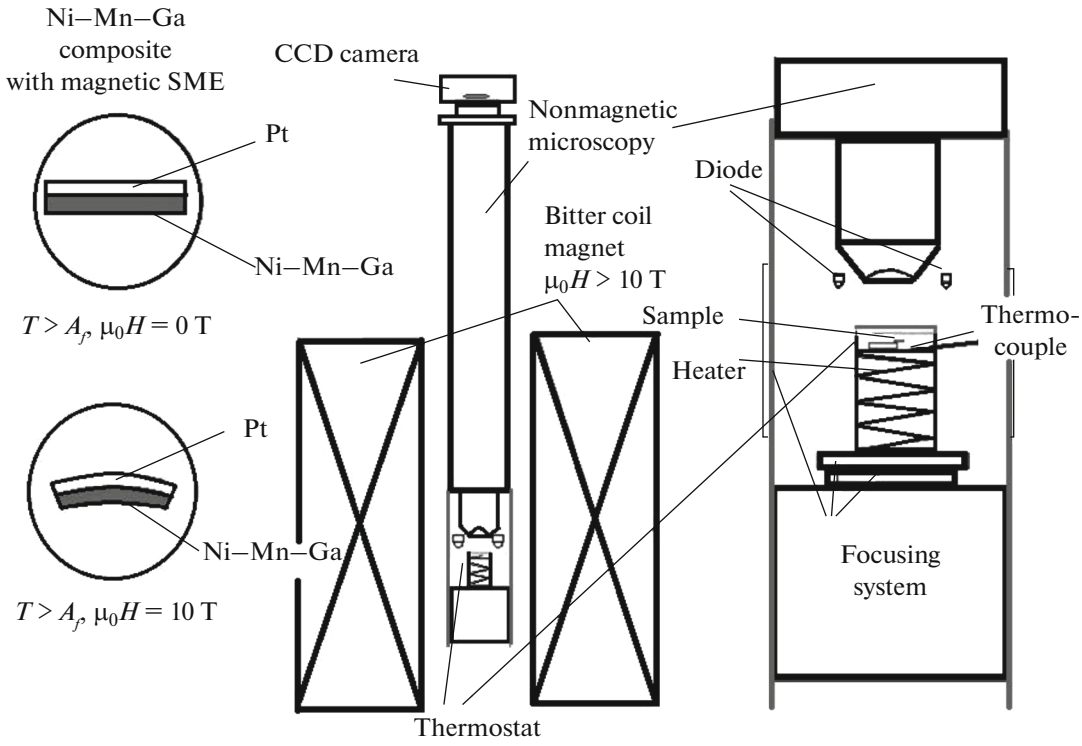

Fig. 9. Scheme of the setup for the study of magnetically induced deformations of the microactuator with SEM.

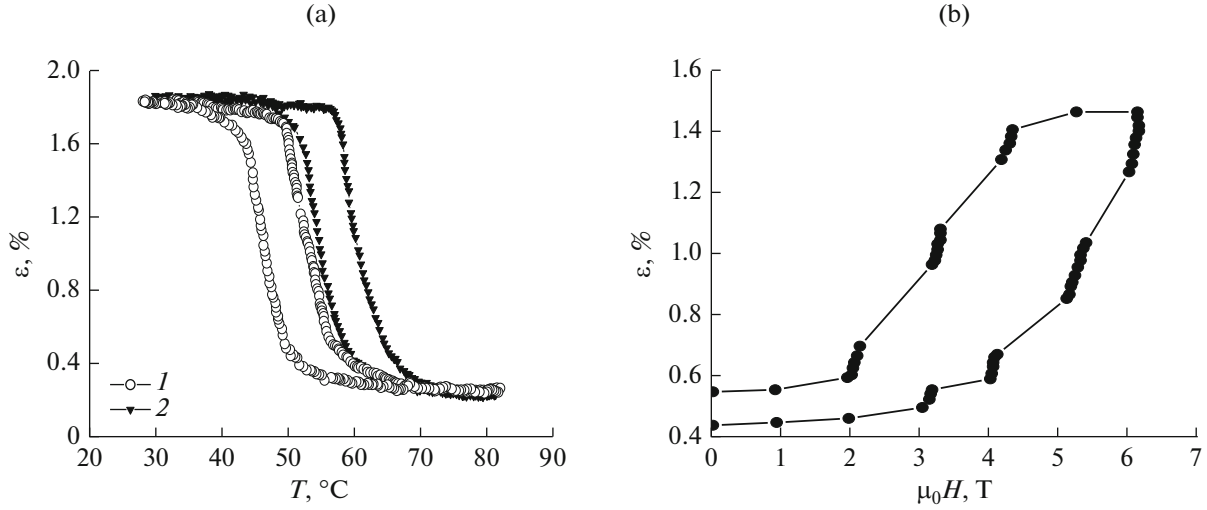

Fig. 10. Thermoeleastic properties of the rapidly quenched $Ni_{53}Mn_{24}Ga_{23}$ in the presence of magnetic field: (a) plot of deformation vs. temperature in the presence of a field of $\mu_0 H =$ (*1*) 6 and (*2*) 0 T and (b) plot of deformation vs. magnetic field at a constant temperature of $T = 56$°C.

bending using formula (1) as in the experiments with the thermally controlled SME.

3. EXPERIMENTAL RESULTS

3.1. One-way SME in the Presence of Thermal and Magnetic Fields

Figure 10a presents the temperature dependences of the deformation of rapidly quenched ribbon made of the $Ni_{53}Mn_{24}Ga_{23}$ Heusler alloy in the presence of a magnetic field of $\mu_0 H = 6$ T and in the absence of the field. It is seen that the hysteresis curve is shifted in the presence of the field toward increasing temperatures by about 56°C. Such a shift is approximately equal to the width of the temperature loop of the hysteresis of the martensite transition. Thus, a reversible martensite transformation with respect to the field and the magnetically controlled reversible deformation of the rib-

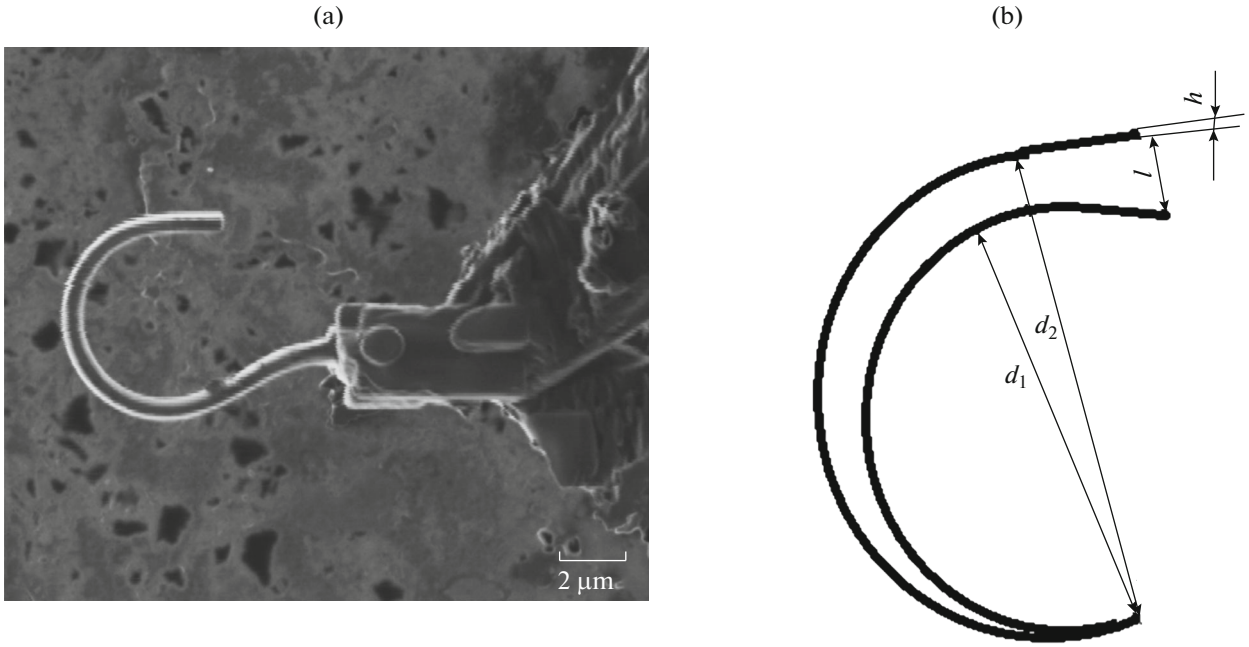

Fig. 11. Two-way SME and superplasticity in the submicron sample of the $Ni_{53}Mn_{24}Ga_{23}$ alloy: (a) martensite state and (b) graphical image of variations in the position of strained sample.

bon due to on–off switching of a field of 6 T can be implemented in practice if the initial temperature of the sample is close to $A_f = 56$°C. Figure 10b shows the deformation versus field at a constant temperature of $T = 56$°C. The reversible magnetically induced deformations are 1.4%. The martensite–austenite and austenite–martensite transformations are obtained for 90% of the sample.

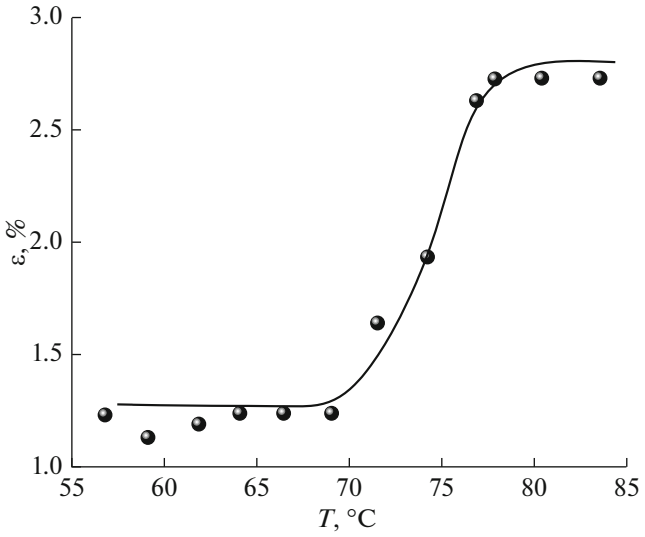

Fig. 12. Plot of relative deformation of composite microactuator ε vs. temperature *T*.

3.2. SME in the $Ni_{53}Mn_{24}Ga_{23}$ Submicron Samples

In the course of manufacturing, a submicron sample is significantly deformed by more than 10%. Even substantially lower deformation leads to the damage of the 3D sample, and, hence, we may conclude that the submicron sample exhibits superplasticity [49].

The experiments on SME in the $Ni_{53}Mn_{24}Ga_{23}$ submicron samples yield the following results. The heating/cooling does not lead to the restoration of the original (linear) shape, which indicates the absence of the one-way shape memory. However, the sample exhibits reversible variation in the relative deformation (i.e., two-way shape memory). Figures 11a and 11b show the sample in the martensite state and a sketch of the deformed sample, respectively. For the two-way SME, the controlled deformation is calculated to be $\Delta\varepsilon \approx 0.5\%$ and the maximum relative deformation of the submicron sample is $\varepsilon \geq 10\%$. Such a deformation is several times greater than the deformation of the original samples with a thickness of about 40 μm. The superplasticity allows training of the rapidly quenched ferromagnetic alloys with submicron sizes that is needed to reach the two-way SME.

3.3. Thermally and Magnetically Controlled SME in the $Ni_{53}Mn_{24}Ga_{23}$/Pt Composite Sample

Dependence $\varepsilon(T)$ (Fig. 12) shows that the controlled bending of the composite sample is no less than $1.5 \pm 0.2\%$. Such a result corresponds to a deflection of 2 μm for the free end of the microactuator.

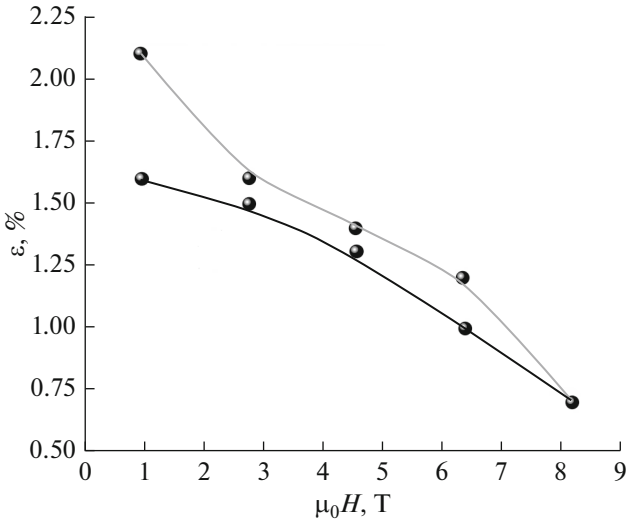

Fig. 13. Plot of relative deformation of composite microactuator ε vs. magnetic field $\mu_0 H$ at a constant temperature of $T = 63°C$.

The study of the magnetically controlled SME shows that the deflection increases with an increase in the magnetic field. At a maximum possible field of $\mu_0 H = 8$ T, the deflection is 1.5 μm and a deformation is no less than 1.8% (Figs. 13 and 14). Note that the sample shape is incompletely recovered in the absence of the magnetic field owing to the fact that the sensitivity of the $Ni_{53}Mn_{24}Ga_{23}$ alloy is insufficient for the complete reversible martensite phase transition at a constant temperature of $T = 63°C$ in the presence of a field of 8 T.

4. DISCUSSION

Metamagnetic Heusler alloys of the Ni–Mn–In, Ni–Mn–Ga, Ni–Mn–Sb, Ni–Mn–Sn, and Ni–Mn–In–Co families are promising for applications in sensor and actuator technology and microsystem technology due to relatively high sensitivity of the martensite transformation and SME to the magnetic field. The corresponding discussion can be found in [12, 25, 50–52] but the problem of randomness of alloy structure that leads to the broadening of the martensite phase transition and a decrease in the sensitivity remains unsolved. The rapidly quenched $Ni_{53}Mn_{24}Ga_{23}$ alloy that has been studied in this work is the best alloy with respect to a combination of the functional and working parameters.

The selective ion etching makes it possible to obtain submicron alloy samples and the corresponding bimorph composites. Unexpectedly, the training of submicron alloy samples easily leads to significant two-way shape memory whereas the one-way shape memory is suppressed. This circumstance can be due to unaccounted effects (e.g., amorphization of the near-surface layer of alloy, which substantially affects the thermomechanical properties).

The experiments show that the layered $Ni_{53}Mn_{24}Ga_{23}$/Pt composites exhibit gigantic thermally and magnetically controlled deformations. Technological solutions and physical conclusions that have been obtained for the Ti_2NiCu/Pt composites in [14, 53] are valid for the composites under study. Deformations of greater than 1% have been obtained due to the on–off switching of the magnetic field at constant temperature close to the room temperature. The magnetically controlled SME can be used to develop devices and instruments that work in natural biological media and make it possible to solve problem of micromanipulation of living biological objects. The problems of material science that remain unsolved are development of an alloy with a relatively high sensitivity to magnetic field and narrow hysteresis of martensite transformation, selection of temperatures of the martensite transition in the vicinity of temperatures of living biological objects, and improvement of functional properties of alloys and composites [54].

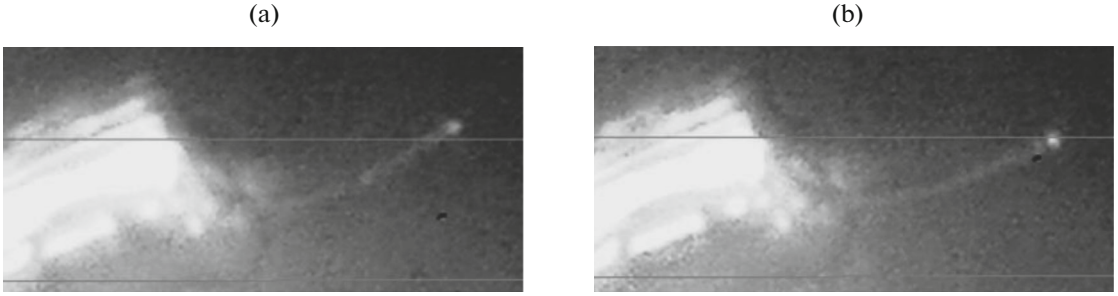

Fig. 14. Experiment on magnetically controlled SME in the optical microscope in the presence of a magnetic field of $\mu_0 H =$ (a) 0 and (b) 8 T at a constant temperature of $T = 63°C$.

CONCLUSIONS

(i) Thermoelastic and magnetomechanical properties of the rapidly quenched $Ni_{53}Mn_{24}Ga_{23}$ alloy have been studied using the dilatometric method, and magnetically controlled SME has been demonstrated in the presence of a Bitter-solenoid field of 8 T.

(ii) The method of the focused ion beam has been used to fabricate submicron samples of the $Ni_{53}Mn_{24}Ga_{23}$ alloy. The submicron samples exhibit superplasticity, and training makes it possible to implement two-way shape memory. The thermally controlled SME has been studied in the chamber of an FEI FIB STRATA 201 ion microscope under diode-laser irradiation.

(iii) The method of the focused ion beam has been employed for fabrication of the $Ni_{53}Mn_{24}Ga_{23}$/Pt composites. Reversible deformations under diode-laser irradiation have been demonstrated for such samples in the chamber of the ion microscope.

(iv) Magnetically controlled deformations of the $Ni_{53}Mn_{24}Ga_{23}$/Pt composites have been observed using the optical method in the presence of a Bitter-solenoid field of up to $\mu_0 H = 8$ T. The reversible deformations are no less than 1.8%.

ACKNOWLEDGMENTS

This work was supported by the Russian Science Foundation (project no. 14-22-00279).

REFERENCES

1. V. D. Buchel'nikov, A. N. Vasil'ev, V. V. Koledov, et al., Physics-Uspekhi **49**, 871 (2006).
2. A. D. Bozhko, A. N. Vasil'ev, V. V. Khovailo, et al., JETP Lett. **67**, 227 (1998).
3. A. D. Bozhko, A. N. Vasil'ev, V. V. Khovailo, et al., J. Exp. Theor. Phys. **88**, 954 (1999).
4. I. Dikshtein, V. Koledov, V. Shavrov, et al., IEEE Trans. Magn. **35**, 3811 (1999).
5. A. Vasiliev, A. Bozhko, V. Khovailo, et al., Phys. Rev. B **59**, 1113 (1999).
6. V. Buchelnikov, I. Dikshtein, R. Grechishkin, et al., J. Magn. Magn. Mater. **272–276**, 2025 (2004).
7. V. V. Kokorin, V. V. Koledov, V. G. Shavrov, et al., J. Appl. Phys. **116**, 103515 (2014).
8. S. Pramanick, S. Chatterjee, S. Giri, et al., J. Alloys Comp. **578**, 157 (2013).
9. L. Gonzalez-Legarreta, T. Sanchez, W. O. Rosa, et al., J. Supercond. Novel Magn. **25**, 2431 (2012).
10. T. Sánchez, R. S. Turtelli, R. Grössinger, et al., J. Magn. Magn. Mater. **324**, 3535 (2012).
11. L. González, J. García, M. Nazmunnahar, et al., Solid State Phenom. **190**, 307 (2012).
12. D. C. Dunand and P. Müllner, Adv. Mater. **23**, 216 (2011).
13. K. Akatyeva, V. Afonina, F. Albertini, et al., Solid State Phenom. **190**, 295 (2012).
14. A. V. Irzhak, V. S. Kalashnikov, V. V. Koledov, D. S. Kuchin, G. A. Lebedev, P. V. Lega, N. A. Pikhtin, I. S. Tarasov, V. G. Shavrov, and A. V. Shelyakov, Tech. Phys. Lett. **36**, 329 (2010).
15. N. I. Kourov, A. V. Korolev, V. G. Pushin, V. V. Koledov, V. G. Shavrov, and V. V. Khovailo, Phys. Met. Metallogr. **99**, 376 (2005).
16. V. G. Pushin, N. I. Kourov, A. V. Korolev, V. A. Kazantsev, L. I. Yurchenko, V. V. Koledov, V. G. Shavrov, and V. V. Khovailo, Phys. Met. Metallogr. **99**, 401 (2005).
17. R. M. Grechishkin, V. V. Koledov, V. G. Shavrov, et al., Int. J. Appl. Electromagn. Mech. **19**, 175 (2004).
18. O. M. Korpusov, R. M. Grechishkin, V. V. Koledov, et al., J. Magn. Magn. Mater. **272–276**, 2035 (2004).
19. A. A. Cherechukin, I. E. Dikshtein, D. I. Ermakov, et al., Phys. Lett. A **291**, 175 (2001).
20. V. A. Chernenko, V. V. Kokorin, and I. N. Vitenko, Smart Mater. Structures **3**, 80 (1994).
21. D. Zakharov, G. Lebedev, V. Koledov, et al., Phys. Procedia **10**, 58 (2010).
22. A. V. Irzhak, D. I. Zakharov, V. S. Kalashnikov, V. V. Koledov, D. S. Kuchin, G. A. Lebedev, P. V. Lega, E. P. Perov, N. A. Pikhtin, V. G. Pushin, I. S. Tarasov, V. V. Khovailo, V. G. Shavrov, and A. V. Shelyakov, J. Commun. Technol. Electron. **55**, 818 (2010).
23. E. Kalimullina, A. Kamantsev, V. Koledov, et al., Phys. Status Solidi C **11**, 1023 (2014).
24. A. Irzhak, V. Koledov, D. Zakharov, et al., J. Alloys Comp. **586**, S464 (2014).
25. M. Kohl, M. Schmitt, A. Backen, et al., Appl. Phys. Lett. **104**, 043111 (2014).
26. V. Bessalova, N. Perov, and V. Rodionova, J. Magn. Magn. Mater. **415**, 66 (2016).
27. F. S. Liu, Q. B. Wang, S. P. Li, et al., Physica B **412**, 74 (2013).
28. Z. Liu, S. Yu, H. Yang, et al., Intermetallics **16**, 447 (2008).
29. H. Feng-Xia, S. Bao-Gen, and S. Ji-Rong, Chin. Phys. B **22**, 037505 (2013).
30. J. L. Sánchez Llamazares, T. Sánchez, J. D. Santos, et al., Appl. Phys. Lett. **92**, 012513 (2008).
31. W. O. Rosa, L. González, J. García, et al., Phys. Res. Int. **2012**, 794171 (2012).
32. D. A. Filippov, V. V. Khovailo, V. V. Koledov, et al., J. Magn. Magn. Mater. (Special Issue) **258**, 507 (2003).
33. V. N. Prudnikov, A. P. Kazakov, I. S. Titov, Ya. N. Kovarskii, N. S. Perov, A. B. Granovsky, I. Dubenko, A. K. Pathak, N. Ali, and J. Gonzalez, Phys. Solid State **53**, 490 (2011).
34. L. González-Legarreta, W. O. Rosa, J. García, et al., J. Alloys Comp. **582**, 490 (2014).
35. T. Sánchez, J. L. Sánchez Llamazares, B. Hernando, et al., Mater. Sci. Forum **635**, 81 (2010).
36. F. Chen, M. Zhang, Y. Chai, et al., Phys. Status Solidi A **209**, 1557 (2012).
37. R. Sahoo, D. M. Raj Kumar, D. Babu Arvindha, et al., J. Magn. Magn. Mater. **347**, 95 (2013).

38. J. Liu, N. Scheerbaum, J. Lyubina, et al., Appl. Phys. Lett. **93**, 102512 (2008).
39. J. Liu, N. Scheerbaum, S. Weiß et al., Appl. Phys. Lett. **95**, 152503 (2009).
40. J. Liu, N. Scheerbaum, D. Hinz, et al., Appl. Phys. Lett. **92**, 162509 (2008).
41. F. Albertini, S. Besseghini, A. S. Bugaev, R. M. Grechishkin, V. V. Koledov, L. Pareti, M. Pasquale, V. G. Shavrov, and D. S. Yulenkov, J. Commun. Technol. Electron. **50**, 638 (2005).
42. N. M. Matveeva, Yu. K. Kovneristyi, L. A. Matlakhova, et al., Izv. AN SSSR, Ser. Metally, No. 4, 97 (1987).
43. F. Albertini, S. Besseghini, A. Paoluzi, et al., J. Magn. Magn. Mater. **242**, 1421 (2002).
44. P. A. Algarabel, C. Magen, L. Morellon, et al., J. Magn. Magn. Mater. **272–276**, 2047 (2004).
45. N. Yao and Ch. L. Van, *The Reference Book on Microscopy for Nanotechnology* (Nauch. Mir, Moscow, 2011) [in Russian].
46. A. Irzhak, V. Koledov, D. Zakharov, et al., J. Alloys Comp. **586**, S464 (2014).
47. D. Zakharov, G. Lebedev, A. Irzhak, et al., Smart Mater. Struct. **21**, 052001 (2012).
48. V. I. Nizhankovskii and V. I. Tsebro, Usp. Fiz. Nauk. **183** (32), 219 (2013).
49. R. Z. Valiev, R. K. Islamgaliev, and I. V. Alexandrov, Progress Mater. Sci. **45**, 103 (2000).
50. E. Pagounis, A. Laptev, J. Jungwirth, et al., Scr. Mater. **88**, 17 (2014).
51. S. Glock, L. P. Canal, C. M. Grize, et al., Composites Sci. Technol. **114**, 110 (2015).
52. Y. Liu, X. Zhang, D. Xing, et al., Physica Status Solidi A **212**, 855 (2015).
53. A. V. Shelyakov, N. N. Sitnikov, V. V. Koledov, et al., Int. J. Smart and Nano Mater. **2** (2), 68 (2011).
54. B. T. Lester, T. Baxevanis, Y. Chemisky, et al., Acta Mechanica **226**, 3907 (2015).

Translated by A. Chikishev